

# On the numerical properties of a wave based prediction technique for coupled vibro-acoustic analysis

W. Desmet, P. Sas, D. Vandepitte

Department of Mechanical Engineering, Division PMA, K.U.Leuven, Belgium

e-mail: wim.desmet@mech.kuleuven.ac.be

## Abstract

A wave based prediction technique for coupled vibro-acoustic analysis has been developed. In contrast with the finite element method, in which the structural and acoustic domains are discretized into small elements and the steady-state dynamic equations are solved within each element using simple, approximate shape functions, the field variable distributions within the entire - or at least large subdomains of the - structural and acoustic domains are approximated in terms of wave functions, which are exact solutions of the homogeneous parts of the dynamic equations. To these wave functions, particular solutions of the inhomogeneous dynamic equations are added, so that the field variable approximations inherently satisfy the dynamic equations exactly. The contributions of the wave functions to the coupled vibro-acoustic response are determined by applying the boundary conditions in a weighted residual formulation.

This paper discusses the numerical condition and convergence properties of the newly developed prediction technique, based on its application for a simple, two-dimensional example. A comparison with the finite element method illustrates that the prediction method has a substantially higher convergence rate, which makes the method applicable for accurate coupled vibro-acoustic predictions up to much higher frequencies.

## 1. Introduction

In the finite element method (FEM), the steady-state dynamic field variables within each element are approximated in terms of shape functions, which are usually based on low-order polynomial functions. Since these functions are no local solutions of the governing dynamic equations, a substantial amount of elements is required in order to accurately represent the oscillatory wave nature of the dynamic response. This results in large models, whose size increases for increasing frequency. Since the subsequent computational effort increases also, the finite element method can only be applied for a limited frequency range. In comparison with uncoupled structural or uncoupled acoustic problems, this practical frequency limit becomes significantly smaller for coupled vibro-acoustic problems, since a structural and an acoustic problem must be solved simultaneously and since the matrices in a coupled FE model are no longer symmetric.

A wave based prediction technique for coupled vibro-acoustic analysis has been developed, based on the indirect Trefftz method [1,2]. The structural and acoustic domains are no longer divided into small

elements. The dynamic field variables in the entire domains, or at least in large subdomains, are expressed in terms of wave functions, which are exact solutions of the homogeneous part of the governing dynamic equations. To these wave functions, particular solutions of the inhomogeneous equations are added, so that the dynamic equations are exactly satisfied a priori. The contributions of the wave functions to the dynamic response are determined by applying the boundary conditions in a weighted residual formulation. Since an approximation is induced only in the representation of the boundary conditions, a high accuracy is obtained from substantially smaller models, compared to the finite element method. In this way, the wave based prediction technique can be applied up to much higher frequencies.

This paper discusses the numerical condition and convergence properties of the wave based prediction technique, based on its application for a simple, two-dimensional example, and illustrates its beneficial performance in comparison with the finite element method.

## 2. Basic principles

### 2.1 Problem definition

A detailed discussion of the wave based prediction technique is given in [3,4]. This paper briefly presents its basic modelling principles, when applied for the two-dimensional coupled vibro-acoustic system, shown in figure 1. One part of the boundary surface of an acoustic cavity consists of a flexible plate with clamped boundaries, while all other parts of the cavity boundary surface are perfectly rigid. The air in the cavity has a density  $\rho_a$  and a speed of sound  $c$ . The plate has a thickness  $t$ , a density  $\rho_s$ , a Poisson coefficient  $\nu$  and an elasticity modulus  $E$ . The acoustic cavity is comprised in an enclosing rectangular domain of size  $L_x \times L_y$ . The coupled vibro-acoustic system is excited by a mechanical line force  $F$ , applied at location  $x_0'$  on the plate, in the direction normal to the plate and with a harmonic time dependence at a certain circular frequency  $\omega$ .

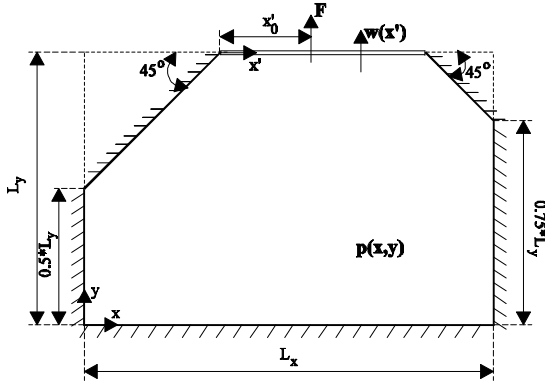


Figure 1: coupled vibro-acoustic system

Since no acoustic sources are present, the steady-state fluid pressure  $p(x,y)$  at each point in the cavity volume  $V$  is governed by the homogeneous Helmholtz equation,

$$\nabla^2 p(x,y) + k^2 \cdot p(x,y) = 0, \quad (x,y) \in V, \quad (1)$$

where  $k(=\omega/c)$  is the acoustic wavenumber. The steady-state normal plate displacement  $w(x')$  of the plate is governed by the inhomogeneous dynamic wave equation,

$$\frac{d^4 w(x')}{dx'^4} - k_b^4 w(x') = \frac{F}{D} \delta(x_0') + \frac{p(x'+0.5L_y, L_y)}{D} \quad (2)$$

where the structural bending wave number  $k_b$  and the plate bending stiffness  $D$  are

$$k_b = \sqrt[4]{\frac{\rho_s t w^2}{D}} \quad \text{and} \quad D = \frac{Et^3}{12(1-\nu^2)}. \quad (3,4)$$

Since the normal fluid velocity must be identical to the normal structural velocity at the fluid-structure coupling interface  $\Omega_s$  and since there can be no fluid velocity, normal to the rigid cavity boundary surface  $\Omega_r$ , the acoustic boundary conditions are

$$\frac{j}{r_a w} \frac{\partial p}{\partial n} = j w w \quad \text{on } W_s, \quad \frac{j}{r_a w} \frac{\partial p}{\partial n} = 0 \quad \text{on } W_r, \quad (5,6)$$

where the normal direction  $n$  has a positive orientation away from the cavity volume  $V$ . The structural clamping boundary conditions are

$$w(0) = w(L_{x'}) = \frac{dw(0)}{dx'} = \frac{dw(L_{x'})}{dx'} = 0, \quad (7)$$

where the plate length  $L_{x'} = L_x - 0.75 \cdot L_y$ .

### 2.2 Solution approximations

The cavity pressure  $p$  is approximated as a solution expansion  $\hat{p}$ ,

$$p(x,y) \approx \hat{p}(x,y) = \sum_{a=1}^{n_a} p_a \cdot F_a(x,y) = [F_a] \{p_a\}. \quad (8)$$

Each function in the  $(1 \times n_a)$  vector  $[F_a]$  is an acoustic wave function, which satisfies eq. (1),

$$F_a(x,y) = e^{-j(k_{xa} \cdot (x - f_{xa} \cdot L_x) + k_{ya} \cdot (y - f_{ya} \cdot L_y))}, \quad (9)$$

$$\text{with} \quad k_{xa}^2 + k_{ya}^2 = k^2. \quad (10)$$

In order to ensure that the amplitudes of the wave functions are not larger than 1 within the acoustic domain, which is beneficial for the numerical condition of the resulting model, the scaling factors  $f_{xa}$  and  $f_{ya}$  are defined as follows,

$$f_a = \begin{cases} 1, & \text{if } \text{Im}(k_a) > 0 \\ 0, & \text{if } \text{Im}(k_a) \leq 0 \end{cases} \quad (a = xa, ya). \quad (11)$$

The contributions of the acoustic wave functions to the solution expansion are comprised in the  $(n_a \times 1)$  vector  $\{p_a\}$ .

The normal plate displacement  $w$  is approximated as a solution expansion  $\hat{w}$ ,

$$w(x') \approx \hat{w}(x') = \sum_{s=1}^4 w_s Y_s(x') + \sum_{a=1}^{n_a} p_a \hat{w}_a(x') + \hat{w}_F(x')$$

$$= [Y_s] \{w_s\} + [\hat{w}_a] \{p_a\} + \hat{w}_F \quad (12)$$

The four wave functions in the  $(1 \times 4)$  vector  $[Y_s]$  are the homogeneous solutions of eq. (2),

$$Y_s(x') = e^{-j^s \cdot k_b \cdot (x' - f_s L_x)}, \quad s = 1..4. \quad (13)$$

Scaling factor  $f_2$  equals 1; the three others are zero. The contributions of the structural wave functions to the solution expansion are comprised in the  $(4 \times 1)$  vector  $\{w_s\}$ .

Function  $\hat{w}_F$  is a particular solution for the mechanical force term in the right-hand side of eq. (2). Several mathematical expressions may serve as particular solution. It is advantageous, however, to select an expression, which is already close to the physical response of the plate. Therefore, the displacement of an infinite plate, excited by a normal line force  $F$  is selected [5],

$$\hat{w}_F(x') = \frac{-jF}{4Dk_b^3} (e^{-jk_b|x'-x_0|} - j \cdot e^{-k_b|x'-x_0|}). \quad (14)$$

The particular solution for the cavity pressure loading term in the right-hand side of eq. (2) may be expressed as an expansion in terms of the functions

$$\hat{w}_a(x') = \frac{F_a(x'+0.5L_y, L_y)}{D \cdot [k_{xa}^4 - k_b^4]}, \quad (15)$$

which are comprised in the  $(1 \times n_a)$  vector  $[\hat{w}_a]$ .

### 2.3 Wave function selection

Since eq. (10) has an infinite number of solutions, a truncated set of acoustic wave functions must be selected. The acoustic wave functions  $\Phi_a$  (see eq. (9)) with the following wavenumber components are selected,

$$(k_{xa}, k_{ya}) = \left( \frac{m_1 p}{L_x}, \pm \sqrt{k^2 - k_{xa}^2} \right)$$

$$\text{and } \left( \pm \sqrt{k^2 - k_{ya}^2}, \frac{m_2 p}{L_y} \right) \quad (16)$$

with  $m_i = 0, \pm 1, \pm 2, \dots$  ( $i=1,2$ ). Recall that  $L_x$  and  $L_y$  are the dimensions of the rectangular domain, enclosing the acoustic cavity. It can be proven [4] that this wave function selection is a T-complete function set [2], in that, in the limit for  $m_1, m_2: 0 \rightarrow \infty$ , the solution expansions (8) and (12) converge towards the exact coupled vibro-acoustic response. Moreover, the contributions of each two acoustic wave functions, whose wavenumber components are based on the same  $m_i$  but with opposite signs, are identical. Hence, the function set for the acoustic expansion (8) may be written as

$$F_a(x, y) = \cos\left(\frac{m_1 p}{L_x} x\right) \cdot e^{-jk_{ya} \cdot (y - f_{ya} L_y)}$$

$$\text{and } \cos\left(\frac{m_2 p}{L_y} y\right) \cdot e^{-jk_{xa} \cdot (x - f_{xa} L_x)} \quad (17)$$

with  $m_i = 0, 1, 2, \dots$  ( $i=1,2$ ).

### 2.4. Integral formulation of the boundary conditions

Due to the particular choice of the solution expansions (8) and (12), the governing dynamic equations (1) and (2) are exactly satisfied, no matter what the values of the wave function contributions  $p_a$  and  $w_s$  are. These contributions are merely determined by the boundary conditions.

The four structural boundary conditions (7) are defined at discrete points of the structural domain and can be used as such. Substitution of the expansions (8) and (12) yields the following matrix form of the structural boundary conditions,

$$[C_{sa} \quad A_{ss}] \begin{Bmatrix} p_a \\ w_s \end{Bmatrix} = \{ \hat{f}_{sF} \}. \quad (18)$$

The  $(4 \times 4)$  matrix  $[A_{ss}]$  results from the application of the differential operators, which are involved with the structural boundary conditions in eq. (7), on the structural wave functions in the  $(1 \times 4)$  vector  $[Y_s]$ ,

$$[A_{ss}] = \begin{bmatrix} \mathbf{Y}_s(0) \\ \mathbf{Y}_s(L_{x'}) \\ \frac{d\mathbf{Y}_s(0)}{dx'} \\ \frac{d\mathbf{Y}_s(L_{x'})}{dx'} \end{bmatrix}. \quad (19)$$

The  $(4 \times n_a)$  coupling matrix  $[C_{sa}]$  results from the application of these differential operators on the particular solution functions in the  $(1 \times n_a)$  vector  $[\hat{w}_a]$ ,

$$[C_{sa}] = \begin{bmatrix} \hat{w}_a(0) \\ \hat{w}_a(L_{x'}) \\ \frac{d\hat{w}_a(0)}{dx'} \\ \frac{d\hat{w}_a(L_{x'})}{dx'} \end{bmatrix}. \quad (20)$$

The  $(4 \times 1)$  vector  $\{\hat{f}_{sF}\}$  results from the particular solution function  $\hat{w}_F$  in (12),

$$\{\hat{f}_{sF}\} = \begin{bmatrix} -\hat{w}_F(0) \\ -\hat{w}_F(L_{x'}) \\ \frac{d\hat{w}_F(0)}{dx'} \\ \frac{d\hat{w}_F(L_{x'})}{dx'} \end{bmatrix}. \quad (21)$$

The acoustic boundary conditions (5,6), which are defined on the entire cavity boundary surface, are transformed into an integral formulation, in which the approximation errors on the boundary conditions are orthogonalized with respect to a weighting function  $\tilde{p}$ ,

$$\int_{W_s} \tilde{p} \cdot \left( \frac{j}{r_{aW}} \frac{\mathcal{I}\tilde{p}}{\mathcal{I}n} - j\mathbf{w}\hat{w} \right) dW + \int_{W_r} \tilde{p} \cdot \left( \frac{j}{r_{aW}} \frac{\mathcal{I}\tilde{p}}{\mathcal{I}n} \right) dW = 0 \quad (22)$$

The weighting function is also expanded in terms of a set of functions  $\tilde{\Phi}_a$ ,

$$\tilde{p} = [\tilde{F}_a] \{\tilde{p}_a\}. \quad (23)$$

Substitution of this weighting function expansion into the integral formulation (22) yields

$$\begin{aligned} & \{\tilde{p}_a\}^T \cdot ([A_{aa}] + [C_{aa}]) \cdot \{p_a\} \\ & + \{\tilde{p}_a\}^T \cdot [C_{as}] \cdot \{w_s\} - \{\tilde{p}_a\}^T \cdot \{\hat{f}_{aF}\} = 0, \end{aligned} \quad (24)$$

where  $^T$  denotes the transpose. The  $(n_a \times n_a)$  matrices  $[A_{aa}]$  and  $[C_{aa}]$  are

$$[A_{aa}] = \frac{j}{r_{aW}} \left( \int_{W_s + W_r} [\tilde{F}_a]^T \left[ \frac{\mathcal{I}F_a}{\mathcal{I}n} \right] dW \right), \quad (25)$$

$$[C_{aa}] = -j\mathbf{w} \left( \int_{W_s} [\tilde{F}_a]^T [\hat{w}_a] dW \right). \quad (26)$$

The  $(n_a \times 4)$  matrix  $[C_{as}]$  is

$$[C_{as}] = -j\mathbf{w} \left( \int_{W_s} [\tilde{F}_a]^T [\mathbf{Y}_s] dW \right) \quad (27)$$

and the  $(n_a \times 1)$  vector  $\{\hat{f}_{aF}\}$  is

$$\{\hat{f}_{aF}\} = j\mathbf{w} \left( \int_{W_s} [\tilde{F}_a]^T \hat{w}_F dW \right). \quad (28)$$

Since the integral formulation (22) should hold for any weighting function  $\tilde{p}$ , the vector  $\{\tilde{p}_a\}^T$  may be eliminated in eq. (24). This yields, in combination with the structural boundary conditions (18), a matrix equation in the unknown wave function contributions  $p_a$  and  $w_s$ ,

$$[A] \begin{Bmatrix} p_a \\ w_s \end{Bmatrix} = \{b\}, \quad (29)$$

$$\text{with } [A] = \begin{bmatrix} A_{aa} + C_{aa} & C_{as} \\ C_{sa} & A_{ss} \end{bmatrix}, \{b\} = \begin{Bmatrix} \hat{f}_{aF} \\ \hat{f}_{sF} \end{Bmatrix}. \quad (30)$$

It can be seen from their definitions that these model matrices are complex, frequency dependent and fully populated.

Several types of functions  $\tilde{\Phi}_a$  may be used in the weighting function expansion (23). Two types of weighting schemes are considered here. In the Galerkin scheme, the acoustic wave functions are used as weighting functions,

$$[\tilde{F}_a] = [F_a]. \quad (31)$$

It can be proven [4] that this scheme yields a symmetric matrix  $[A_{aa}]$ . The weighting scheme, for which

$$[\tilde{F}_a] = \begin{bmatrix} \mathcal{I}F_a^* \\ \mathcal{I}n \end{bmatrix}, \quad (32)$$

and where  $*$  denotes the complex conjugate, is referred to as a least-squares weighting scheme, since each row in that part of matrix equation (29), that originates from eq. (24), corresponds with

$$\frac{\mathcal{I}F}{\mathcal{I}p_a} = 0, \quad (33)$$

with

$$F = \int_{W_s} \left\| \frac{j}{r_a w} \frac{\mathcal{I}p}{\mathcal{I}n} - jw\hat{w} \right\|^2 dW + \int_{W_r} \left\| \frac{j}{r_a w} \frac{\mathcal{I}p}{\mathcal{I}n} \right\|^2 dW.$$

Note, however, that the dependence of the structural displacement approximation  $\hat{w}$  on the wave function contributions  $p_a$  (see eq. (12)) is only taken into account in the evaluation of the functional  $F$ , but not in the evaluation of its derivatives in eq. (33). For this least-squares weighting scheme, the matrix  $[A_{aa}]$  becomes Hermitian. The convergence properties of the two weighting schemes are compared in section 4.1.

### 3. Numerical condition

As it is the case for any type of Trefftz implementation [6], the wave model (29) has a poor numerical condition, in that the ratio between the largest and smallest singular value of matrix  $[A]$  is large. However, in contrast with the other, currently available T-complete function sets [2,7,8], the proposed function set (17) yields a system model, whose poor numerical condition is not preventing the prediction results from converging towards the exact solutions. This may be seen, for instance, from a Picard test of the system model [9,10]. The singular value decomposition of matrix  $[A]$  takes the form

$$[A] = [U][S][V]^H = \sum_{i=1}^{n_a+4} \{U_i\} \cdot s_i \cdot \{V_i\}^H, \quad (34)$$

where  $[\Sigma]$  is a diagonal matrix of singular values  $\sigma_i$ , where  $\{U_i\}$  and  $\{V_i\}$  are the  $i$ -th column vectors of the orthonormal matrices  $[U]$  and  $[V]$  and where  $^H$  denotes the complex conjugate transpose. The solution of matrix equation (29) may then be written as

$$\begin{Bmatrix} p_a \\ w_s \end{Bmatrix} = \sum_{i=1}^{n_a+4} \frac{\{U_i\}^H \cdot \{b\}}{s_i} \{V_i\} = \sum_{i=1}^{n_a+4} \frac{b_i}{s_i} \{V_i\}. \quad (35)$$

When a matrix has a poor numerical condition, it has several very small singular values. As may be seen from eq. (35), the solution vector is then usually dominated by the terms, which correspond with the very small singular values and yields useless, non-converging results. However, if the coefficients  $\beta_i$ , associated with those very small singular values, are also very small, reliable, converging results may be obtained. In a Picard test, the singular values  $\sigma_i$  are compared with their associated coefficients  $\beta_i$ . When the latter are smaller or at least not very much larger than their associated singular values, the problem is said to be mildly ill-conditioned, indicating that reliable results may be obtained. This is the case for the proposed wave model, as illustrated in figure 2, which plots the amplitudes of the singular values  $\sigma_i$  against the amplitudes of the coefficients  $\beta_i$  for  $n_a=150$ .

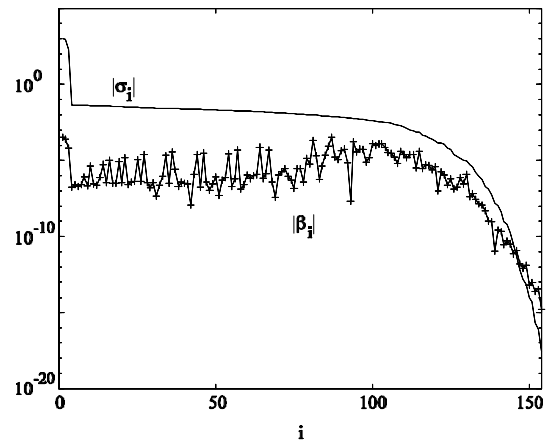


Figure 2: Picard test

Hence, according to this Picard test, convergence of the prediction technique may be expected, despite the poor numerical condition.

## 4. Convergence

### 4.1 Validation example

The wave model (29) has been solved for the case of an air-filled ( $\rho_a=1.225\text{kg/m}^3$ ,  $c=340\text{m/s}$ ) cavity ( $L_x=1.5\text{m}$ ,  $L_y=1\text{m}$ ) and an aluminium ( $E=70.10^9\text{N/m}^2$ ,  $\rho_s=2790\text{kg/m}^3$ ,  $\nu=0.3$ ,  $t=2.10^{-3}\text{m}$ ) plate. A unit normal line force  $F$  is applied at  $x_0'=0.5\text{m}$ .

Since the solutions expansions (8) and (12) inherently satisfy the governing dynamic equations, it is sufficient to check the representation of the boundary conditions in order to assess the prediction accuracy of a wave model. Figure 3 plots the instantaneous normal structural displacement  $w$  against the fluid displacement  $w_a$ , normal to the fluid-structure coupling interface, at 200 Hz, obtained from a wave model with  $n_a=300$ . This figure clearly indicates the accurate representation of the displacement continuity condition in eq. (5) and the clamped boundary conditions in eq. (7).

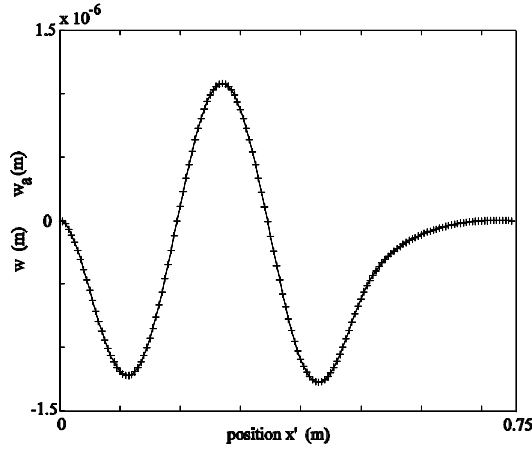


Figure 3: instantaneous normal structural (solid line) and fluid (+) displacement at the coupling interface at 200 Hz

The corresponding instantaneous cavity pressure is shown in figure 4. The fact that the pressure contour lines are perpendicular to all rigid parts of the cavity boundary surface, indicates that the acoustic boundary condition in eq. (6) is accurately represented. From these figures, it may be concluded that the proposed wave model converges towards the exact solution.

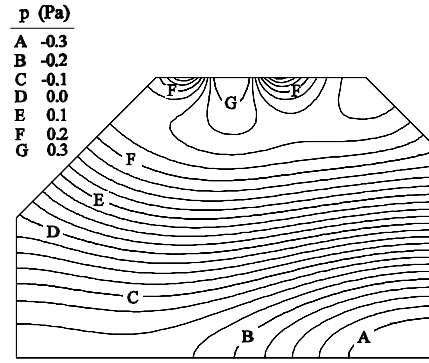


Figure 4: contour plot of the instantaneous cavity pressure at 200 Hz

Another indication of the convergence of the wave based prediction technique is given by the convergence curve, which plots the prediction error  $\Delta\varphi$  on a field variable  $\varphi$  against the size of the wave model, i.e. the number of degrees of freedom  $n_a+4$ . The prediction error may be defined as

$$Dj = \frac{\|j - j_\infty\|}{\|j_\infty\|}, \quad (36)$$

where  $\varphi$  is the predicted field variable value and  $\varphi_\infty$  is its exact value. Since the exact solution is not known, the prediction error is evaluated, using the prediction result, obtained from a very large model, as  $\varphi_\infty$ . If the wave model converges to the exact solution, the prediction error should tend to zero for increasing model sizes. Figure 5 plots the convergence curves for the normal plate displacement at  $x'=0.25\text{m}$  and for the cavity pressure at  $(x,y)=(0.5\text{m},0.5\text{m})$  at 200 Hz and 500 Hz.

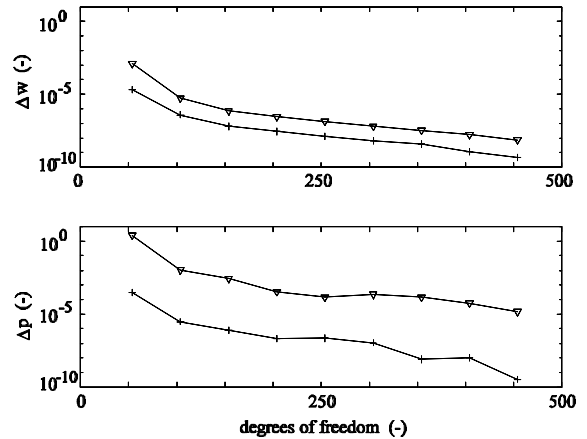


Figure 5: structural (upper part) and acoustic (lower part) convergence curves at 200 Hz (+) and 500 Hz (v)

These curves confirm again the convergence of the proposed wave model.

Figure 6 compares the convergence curves for the normal plate displacement at  $x'=0.25\text{m}$  at 200 Hz and 500 Hz, obtained from the Galerkin and the least-squares weighting schemes (31) and (32). This figure clearly indicates the beneficial convergence rate of the Galerkin weighting scheme.

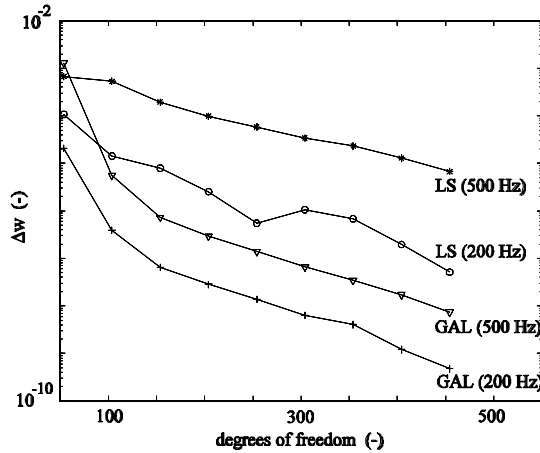


Figure 6: convergence curves for Galerkin (GAL) and least-squares (LS) weighting schemes

## 4.2 Comparison with FEM

The results from the wave based prediction technique have been compared with the results from several finite element models. The latter results were obtained from the MSC/NASTRAN software. A two-dimensional element discretization was obtained from one three-dimensional layer of 8-noded hexahedral fluid elements and 4-noded quadrilateral shell elements, in which the invariance in the third dimension was modelled with the appropriate multiple point constraints. Table 1 lists the number of elements of each FE model and their corresponding unconstrained degrees of freedom.

	# str. elem.	# ac. elem.	dof
model 1	36	3056	3682
model 2	54	7776	8116
model 3	108	31104	31786
model 4	135	48600	49453

Table 1: properties of the FE models

Since an approximation error is induced only on the boundary conditions, a wave model has a substantially smaller size than a corresponding FE

model. However, the beneficial effect of a smaller model size on the computational effort is partly annihilated by some disadvantageous matrix properties: in contrast with the FE method, the wave based prediction technique yields fully populated, complex and frequency dependent matrices. Therefore, it is more appropriate for convergence comparisons to plot the prediction error against the corresponding CPU time, instead of the number of unconstrained degrees of freedom. Figure 7 shows these convergence curves for the normal plate displacement at  $x'=0.25\text{m}$  and for the cavity pressure at  $(x,y)=(0.5\text{m},0.5\text{m})$  at 200 Hz and 500 Hz. The plotted CPU times denote the CPU times, needed for the response calculation at one frequency on a HP-C180 workstation (SPECfp95=18.7, SPECint95=11.8). The CPU time for the wave models includes both the time for constructing the model as well as solving the resulting matrix equation, while the CPU time for the FE models comprises only the solution time.

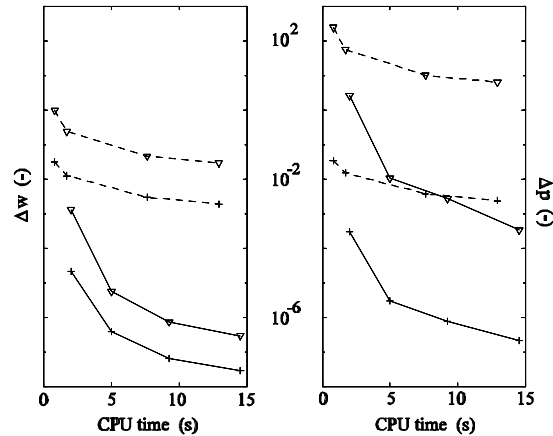


Figure 7: structural (left part) and acoustic (right part) convergence curves at 200 Hz (+) and 500 Hz (∇) (solid: wave based prediction technique, dashed: FEM)

This figure clearly indicates the advantageous computational efficiency of the wave based prediction technique in comparison with the finite element method. Moreover, this improved efficiency will most likely become even more apparent, when the technique is implemented in an efficient programming environment, instead of the currently used MATLAB environment.

## 5. Conclusions

A wave based prediction technique for coupled vibro-acoustic analysis has been developed. The technique is based on the indirect Trefftz method and approximates the structural and acoustic field variables of a coupled vibro-acoustic system in terms of solution expansions, which exactly satisfy the governing dynamic equations. The contribution factors in these expansions are obtained from a weighted residual formulation of the boundary conditions.

This paper discusses the numerical condition and convergence properties of the wave based prediction technique, based on its application for a simple, two-dimensional example. As it is the case for any type of Trefftz implementation, the system models of the wave based prediction technique have a poor numerical condition. However, a particular type of solution expansion has been found, which yields a system model, whose poor numerical condition is not preventing the prediction results from converging towards the exact solutions. The convergence rate is strongly dependent on the type of weighted residual formulation of the boundary conditions. In this respect, a Galerkin weighted residual formulation is preferred to a least-squares formulation.

A comparison with some corresponding finite element models illustrates that highly accurate prediction results may be obtained with a substantially smaller computational effort. Due to this beneficial convergence rate, the practical frequency limit for the wave based prediction technique may become substantially higher than for the finite element method.

## References

1. E. Trefftz, *Ein Gegenstück zum Ritzschen Verfahren*, Proc. 2nd Int. Cong. Appl. Mech (Zurich, 1926), 131-137.
2. E. Kita, N. Kamiya, *Trefftz method: an overview*, Advances in Engineering Software, **24**, 3-12 (1995).
3. W. Desmet, P. Sas, D. Vandepitte, *A new wave based prediction technique for coupled vibro-acoustic analysis: theoretical description and application to a double wall structure*, Proc. ISMA 21 (Leuven, 1996), 105-134.

4. W. Desmet, *A wave based prediction technique for coupled vibro-acoustic analysis*, PhD dissertation, K.U.Leuven, 1998 (to appear).
5. M.C. Junger, D. Feit, *Sound, Structures and Their Interaction*, (The MIT Press, Cambridge, Massachusetts, London, 1972).
6. A.P. Zielinski, I. Herrera, *Trefftz method: fitting boundary conditions*, Int. J. Num. Meth. Eng. **24**, 871-891 (1987).
7. P. Masson, E. Redon, J.-P. Priou, Y. Gervais, *The application of the Trefftz method to acoustics*, Proc. of the Third International Congress on Air- and Structure-borne Sound and Vibration (Montreal, 1994), 1809-1816.
8. R.S. Langley, *Some perspectives on wave-mode duality in SEA*, IUTAM Symposium on Statistical Energy Analysis (Southampton, 1997).
9. J.M. Varah, *A practical examination of some numerical methods for linear discrete ill-posed problems*, SIAM Rev. **21**, 100-111 (1979).
10. J.M. Varah, *Pitfalls in the numerical solution of linear ill-posed problems*, SIAM J. Sci. Stat. Comput. **4**, 164-176 (1983).